REPORT DOCUMENTATION PAGE

AFRL-SR-AR-TR-02-

0238

1. REPORT DATE (DD-MM-YYYY)	2. REPORT TYPE	3. DATES COVERED (From - To)
01-07-2002	Final Technical Report	Sept. 1998-March 2002

4. TITLE AND SUBTITLE
Sol-Gel Derived Surface Treatments for Aircraft Aluminum Alloys

5a. CONTRACT NUMBER
F49620-98-1-0502 98-1-6502

5b. GRANT NUMBER

5c. PROGRAM ELEMENT NUMBER
61103D

6. AUTHOR(S)
Knobbe, Edward T.

5d. PROJECT NUMBER
3484

5e. TASK NUMBER
BS

5f. WORK UNIT NUMBER

7. PERFORMING ORGANIZATION NAME(S) AND ADDRESS(ES)

Oklahoma State University
Environmental Institute
003 Life Sciences East
Stillwater, OK 74078-3011

8. PERFORMING ORGANIZATION REPORT NUMBER

9. SPONSORING / MONITORING AGENCY NAME(S) AND ADDRESS(ES)

Air Force Office of
Scientific Research /NL
801 N. Randolph Street,Rm 732
Arlington, VA 22203-1977

10. SPONSOR/MONITOR'S ACRONYM(S)
AFOSR/NL

11. SPONSOR/MONITOR'S REPORT NUMBER(S)

12. DISTRIBUTION / AVAILABILITY STATEMENT

Approved for public release; distribution is unlimited

20020816 064

13. SUPPLEMENTARY NOTES

14. ABSTRACT

Technologies for providing enhanced corrosion resistance for 2024-T3 aluminum alloy were investigated. This program investigated (a) laser processing of metal surfaces to obtain optimum corrosion resistance and (b) the development of sol-gel derived coatings specifically targeted for use on aircraft aluminum alloys. Specifically, a nanosecond excimer laser was used for the surface modification of structure and composition of 2024-T3 aluminum alloy. Environmental scanning electron microscopy (ESEM) was used to characterize the alloy surface structural modification and composition as a function of laser fluence and pulse number. Potentiodynamic scan (PDS) and electrochemical impedance spectroscopy (EIS) were used to analyze corrosion resistance properties of the pre- and post-treated alloys. The ablation process was found to result in the removal of second phase elements, i.e. copper, and growth of the barrier aluminum oxide layer on the surface. These two complementary effects were found to enhance the corrosion resistance properties of the aluminum alloy surface. Additionally, various organically-modified silicate (Ormosil) coatings were investigated and found to provide good corrosion resistance characteristics for 2024-T3 aluminum alloys as determined using potentiodynamic polarization scans and accelerated salt spray testing. Ormosil structures were investigated using solid state NMR. Structure/property relationships were developed based on a correlation of NMR and salt spray/electrochemical data. The incorporation of a curing agent was found to enhance the corrosion resistance characteristics of the Ormosil coating.

15. SUBJECT TERMS
Corrosion resistance, sol-gel derived coatings

16. SECURITY CLASSIFICATION OF:			17. LIMITATION OF ABSTRACT	18. NUMBER OF PAGES	19a. NAME OF RESPONSIBLE PERSON
a. REPORT	b. ABSTRACT	c. THIS PAGE		38	Elizabeth M. McTernan
					19b. TELEPHONE NUMBER (include area code) 405-744-9996

Sol-Gel Derived Surface Treatments for Aircraft Aluminum Alloys

Principle Investigator: Dr. Edward T. Knobbe
Oklahoma State University

Abstract

Technologies for providing enhanced corrosion resistance for 2024-T3 aluminum alloy were investigated. This program investigated (a) laser processing of metal surfaces to obtain optimum corrosion resistance and (b) the development of sol-gel derived coatings specifically targeted for use on aircraft aluminum alloys. Specifically, a nanosecond excimer laser was used for the surface modification of structure and composition of 2024-T3 aluminum alloy. Environmental scanning electron microscopy (ESEM) was used to characterize the alloy surface structural modification and composition as a function of laser fluence and pulse number. Potentiodynamic scan (PDS) and electrochemical impedance spectroscopy (EIS) were used to analyze corrosion resistance properties of the pre- and post-treated alloys. The ablation process was found to result in the removal of second phase elements, i.e. copper, and growth of the barrier aluminum oxide layer on the surface. These two complementary effects were found to enhance the corrosion resistance properties of the aluminum alloy surface. Additionally, various organically-modified silicate (Ormosil) coatings were investigated and found to provide good corrosion resistance characteristics for 2024-T3 aluminum alloys as determined using potentiodynamic polarization scans and accelerated salt spray testing. Ormosil structures were investigated using solid state NMR. Structure/property relationships were developed based on a correlation of NMR and salt spray/electrochemical data. The incorporation of a curing agent was found to enhance the corrosion resistance characteristics of the Ormosil coating.

Publications Stemming from this Research Effort

1. "Enhancement of Corrosion Resistance Characteristics of 2024-T3 Aluminum Alloy Through Laser-Induced Surface Modification," Olga Kachurina, Tammy L. Metroke, and Kai Dou, in preparation, to be submitted to *Journal of Laser Applications*.

2. "Comparison of Single and Multilayer Coatings Based on Ormosil and Conversion Layers for Aluminum Alloy Corrosion Inhibition," Olga Kachurina, Tammy L. Metroke, Elvira Stesikova and Edward T. Knobbe – *Journal of Coatings Technology*, 74 (2002) 43-48.

3. "Electrochemical and Salt Spray Analysis of Multilayer Ormosil/Conversion Coating Systems for Corrosion Resistance of 2024-T3 Aluminum Alloy", Tammy L. Metroke, Olga Kachurina, and Edward T. Knobbe, *Journal of Coatings Technology*, 74 April (2002) 53-61.

4. "Impact of Trivalent Chromium Conversion Layers and Hybrid Silicate Coatings on Corrosion Resistance of Aluminum Alloys" E. Stesikova, T. Metroke, P. Reed, V. Agarwala, E. Knobbe; Proceedings Paper #287 in Corrosion NACE 2000 Annual Meeting, March 2000, Orlando Florida.

5. "Organic-Inorganic Hybrid Coatings as Corrosion Inhibiting Surface Treatments for Aluminum Alloys"; T.L. Metroke, E. Stesikova, O. Kachurina, E. Knobbe; Proceedings Paper #01550 in Corrosion NACE 2001 Annual Meeting, March 2001, Houston, Texas.

6. "Trivalent Chromium/Organically-Modified Silicate Composite Coatings for Corrosion Protection of Aluminum Alloys" E. Stesikova, T. Metroke, O. Kachurina, E. Knobbe; 4th Conference on Aerospace Materials, Processes, and Environmental Technology, Van Braun Center, Huntsville, Alabama, Sept. 18-20, 2000.

7. "Composite Coatings Based on Hybrid Silicate and Trivalent Chromium Conversion Layers for Aluminum Alloy Corrosion Inhibition" T. Metroke, O. Kachurina, E. Stesikova, E. Knobbe; ACS Meeting, Washington DC, August 2000.

8. "Corrosion Resistance Properties of Organic-Inorganic Hybrid Materials on Aluminum Alloys Using Salt Spray Techniques" T. Metroke, E. Stesikova, E. Knobbe, R. Parkhill, M. Donley; Aging Aircraft 2000, May 2000, St. Louis, Missouri.

I. Laser Surface Treatment of 2024-T3 Aluminum Alloy

A. Introduction

Various surface treatments such as anodizing, conversion coating, and application of organic polymer paint systems can be used to improve protective and decorative properties of aluminum alloys. In the anodic oxidation of aluminum alloy, also called anodizing, the metal is connected as an anode in an electrolytic cell containing a suitable electrolyte, for example, borate or tartrate solutions. Electrochemical aluminum oxidation takes place and the formed aluminum cations react with oxygen anions of the aqueous electrolyte to form aluminum oxide. The structure and composition of the oxide layer depend on the electrolyte nature, the electrolysis parameters (i.e. current density, potential and process time) and the composition of the treated aluminum surface. If the natural oxide film is insoluble in the electrolyte, film thickening is observed resulting in a compact, strongly-adherent, non-conducting film. The thickness of the barrier layer generally is in the 0.01 μm – 1 μm range and varies directly with the forming voltage[1].

Significant work aimed at the modification of surface compositions and/or morphologies, such as ablation, surface cleaning and hardening, phase transformations, thin film deposition, surface alloying, melting and cladding, micromachining and microstructuring, have all been demonstrated using pulsed laser sources to irradiate solid state specimens. Temporally short laser pulses, such as those produced by excimer lasers, provide a mechanism for the alteration of surface morphology or structure without significant damage to or perturbation of the underlying material. Unique material surface compositions or surface structures may be achieved through the controlled use of the available irradiation parameters of the pulsed laser, such as wavelength, pulse energy, fluence, repetition rate, and pulse count. Thus, it is possible to develop unique

phases, surface compositions, and/or surface microstructures through the appropriate combination of laser processing parameters[2].

In this work, a nanosecond excimer laser was used for the surface modification of structure and composition of 2024-T3 aluminum alloy. Environmental scanning electron microscopy (ESEM) was used to characterize the alloy surface structural modification and composition as a function of laser fluence and pulse number. Potentiodynamic scan (PDS) and electrochemical impedance spectroscopy (EIS) were used to analyze corrosion resistance properties of the pre- and post-treated alloys. The ablation process was found to result in the removal of second phase elements, i.e. copper, and growth of the barrier aluminum oxide layer on the surface. These two complementary effects were found to enhance the corrosion resistance properties of the aluminum alloy surface.

B. Experimental

1. Nanosecond-Pulse Irradiation

An excimer laser delivering 15 ns pulses at 308 nm was employed for nano- and microscale surface morphology and composition experiments. The pulse output energy was measured using a Molectron J - 50 joulemeter probe connected to a Tektronics TDS640A oscilloscope. Maximum energy output was found to be 320 mJ for nanosecond pulses. A fused silicon lens with focal length of 30 cm was used to focus the laser beam on the sample surface. Location of the laser irradiation spot on the sample was varied using a translation stage. Each sample was irradiated with 10-1000 pulses using a repetition rate of 10 Hz. Variable spot sizes were used to produce irradiation fluences ranging from 0.02 to 5.0 J/cm^2. The morphology of the

ablated area was characterized by a Leica-Cambridge Stereoscan 360 FE electron microscope operating at 15 kV with a working separation of 10 mm. The elementary analysis was achieved by using an environmental scanning electron microscope (ESEM); the resolution of this instrument is 0.1 wt. %.

2. Potentiodynamic Scan and Electrochemical Impedance Spectroscopy

Potentiodynamic scans (PDS) and electrochemical impedance spectroscopy (EIS) were used to evaluate the corrosion protective properties of investigated laser-treated aluminum alloy (AA) surface. Detailed descriptions of these electrochemical methods can be found elsewhere[3]. Each coating system was evaluated in triplicate. Electrochemical measurements were performed using a Gamry PC3/300 potentiostat with Gamry Corrosion Measurement System DC105 and EIS300 software. A three electrode cell equipped with a platinum counter electrode, a $Ag/AgCl/Cl^-$ (3M KCl) reference electrode and the laser-treated 2024-T3 AA panel as the working electrode; an exposed area of 0.36 cm^2 was used for all experiments. All measurements were conducted in dilute Harrison's solution (0.35 wt% $(NH_4)_2 SO_4$ and 0.05 wt% NaCl) at 25 ± 1 °C. This mixture of electrolytes is considered to closely emulate atmospheric environment for aircraft[4]. Coatings were immersed in dilute Harrison's solution 15 minutes prior to the test. The reported values of potentials shown in the polarization curves and listed in the tables are given relative to the $Ag/AgCl/Cl^-$ reference electrode. Potentiodynamic scans were acquired in the region from –50 mV vs E_{oc} (open circuit potential) to pitting potential. Pitting potentials, E_{pit}, were determined using the criterion described by Kelly et al wherein pitting would have occurred by the time the anodic current density of the specimen reached 3×10^{-5} A/cm^2 [(5)].

EIS tests were performed in triplicate on a Gamry PC3/300 potentiostat using a Gamry Corrosion Measurement System CMS100 and CMS300 software. Coatings were immersed in dilute Harrison's solution 30 minutes before data acquisition. The electrode arrangement is identical to the PDS cell set up described above. EIS spectra were acquired in the frequency range from 10 kHz to 10 mHz with 10 mV-applied ac (vs. E_{oc}). Standard coating analysis criteria are as follows: Impedance values, $|Z|$, above $1x10^9$ Ωcm^2 are indicative of coatings with excellent barrier properties. Coatings with $|Z|$ values between $1x10^6$ and $1x10^9$ Ωcm^2 are considered to be good barrier coatings. Coatings with impedance values below $1x10^6$ Ωcm^2 are considered to be poor barrier coatings[6].

PDS was used to define important characteristics including corrosion potential, E_{corr}, and pitting potential, E_{pit}. Corrosion current, I_{corr}, and corrosion resistance, R_{corr}, were defined using Gamry software using the polarization resistance method. R_{corr} is defined as the slope of the current density-potential curve at the corrosion potential, as per ASTM G3-89. I_{corr} is defined as $20mV/R_{corr}$.

C. Results and Discussion

1. Surface Structuring and Composition as a Function of Nanosecond Pulse Irradiation

In this study, the laser ablation experiment was designed to investigate the effects on corrosion resistance properties of removing or reducing the surface alloying elements that are originally incorporated in the aluminum alloy for the purpose of improving mechanical and electrical properties. Corrosion resistance characteristics were investigated as a function of pulse

number and laser fluence. We anticipate that removal of the alloying elements will lead to an enhancement of corrosion resistance characteristics by removing active sites for corrosion initiation, i.e. copper inclusions.

Figure 1 shows the SEM images of the surface modification produced by irradiation using 1000 pulses with fluences in the range of 0.8 - 3.0 J/cm^2. Careful examination indicates that irradiation under these conditions generates significant surface modification, especially at fluences $\geq$ 1.2 J/cm^2 as shown in Fig. 1 (b) and (c). As shown in the Figure, the alloy was found to exhibit threshold behavior for surface structure as a function of fluence. As the irradiating fluence approached the fluence value of 1.2 J/cm^2 for ablation in aluminum, surface texturing effects are observed and surface features ranging from several micron down to submicron dimensions become widespread. As the ablation process continues, the melt structure develops as a function of increasing laser fluence.

Figure 2 shows ESEM calculations of the percentage of copper in the aluminum alloy as a function of laser fluence. Initial analysis indicates that the as-received 2024-T3 aluminum alloy contains 4.4 wt. % copper. Surface treatment using fluences in the 0.8-0.9 J/cm^2 range resulted in a reduction in the copper concentration on the alloy surface. Laser surface treatment using fluences of 1.0-1.3 J/cm^2 produced a reduction in the copper concentration identified by the ESEM to approximately 1.0 wt. %. The composition analysis also indicates that the concentrations of magnesium and manganese are only marginally altered by the laser ablation. As the applied fluence is elevated to 1.8 J/cm^2, the copper composition was found to increase to 4.12 wt. %. This behavior is expected due to migration of copper atoms from the bulk metal to the alloy surface. These results indicate that for moderate fluences, 1.0 – 1.3 J/cm^2, it is possible to preferentially reduce the copper concentration on the metal surface using laser irradiation;

laser surface treatment provides a powerful means of surface composition modification in a controlled manner through variation of both laser fluence.

2. Corrosion Resistance Characteristics of Laser-Irradiated 2024-T3 AA Surfaces

Corrosion resistance characteristics of laser-irradiated surfaces were analyzed using electrochemical methods including the polarization resistance method, potentiodynamic polarization scan (PDS), and electrochemical impedance spectroscopy (EIS). These methods provide a quantitative description of corrosion resistance characteristics of the modified surfaces. The model used for surface analysis using EIS was the Randel model, which is commonly used for the analysis of barrier film properties of anodized coatings[7]. The equivalent circuit used to model experimental data is presented in Figure 3. In the model and the experimental data, R_{pol} denotes polarization resistance, R_u denotes solution resistance, and C_{dl} denotes double layer capacitance.

Figure 4 represents a typical Bode plot for the 2024-T3 AA surface after laser treatment using a fluence of 1.2 J/cm^2. The surface produced by laser treatment generally exhibited very high impedance values at low frequencies. The approach of the phase angle component to –90° at low frequencies is indicative of the formation of a dense, protective coating on the metal surface after laser treatment. Considering that the ablation experiment was performed in air, we anticipate that the high phase angle component indicates the growth of a dense aluminum oxide surface layer.

Electrochemical characteristics of $K_2Cr_2O_7$ on 2024-T3 AA was chosen as a control system due to its use as the active ingredient in standard military and industrial corrosion

resistance pretreatment for aluminum alloys. Tables 1 and 2 show electrochemical characteristics for laser-treated test pieces derived from PDS and EIS analyses, respectively.

3. Corrosion Resistance Properties as a Function of Number of Laser Pulses

Surface modification with 10-500 pulses (308 nm, 15 ns) with a fluence of 1.2 J/cm^2 was not found to produce a significant modification to the corrosion resistance characteristics of the aluminum alloy surface as determined using EIS. Despite increases in R_{pol} with increasing pulse number at constant fluence, a significant corrosion protection was not observed, as the R_{pol} values were in the range (278-469) kΩcm^2 compared to 1590 kΩcm^2 for hexavalent chromium coating. The increase of R_{pol} with the surface modification using laser irradiation with the fluence 1.2 J/cm^2 and small number of pulses (20-500) could be explained as growth of a very thin aluminum oxide layer on the metal surface.

Further indication of the growth of an oxide film on the AA surface is a decrease in the value of C_{dl}. The decrease in double layer capacity extracted from the Randell model from 10 μF/cm^2 for bare aluminum covered with natural oxide film to 7 μF/cm^2 for 1.2 J/cm^2 and 20 pulses laser treated aluminum alloy surface and further to 4 μF/cm^2 for all samples treated in the range (50-500) pulses at the same fluence is indicative of growing aluminum oxide layer on the AA surface. Assuming that the composition of the growing aluminum oxide layer remains constant for all fluences, the difference in thickness of this layer is inversely related to C_{dl}, taking into consideration that $C_{coat} = (e \times e_0 \times A)/d$, where e denotes the relative dielectric constant, e_0 denotes the absolute dielectric constant of vacuum, 8.85×10^{-12} F m^{-1}, A denotes the electrode surface area, and d denotes the coating thickness[8]. Observed E_{corr} and E_{pit} values for AA samples treated with the laser irradiation in the range (50-500) pulses using 1.2 J/cm^2 fluence, were found

in the very narrow range (0.650-0.695) V and (–0.22 –0.28) V, respectively. Analogously, the R_{pol} data extracted from the PDS for the same samples are in the narrow range of (291-469) $k\Omega cm^2$ and indicate their similar corrosion protective properties, which are significantly lower than 1500 $k\Omega cm^2$ observed for hexavalent chromium conversion coating.

4. Corrosion Resistance Properties as a Function of Laser Fluence

Surface modification with 1000 pulses at 308 nm with a pulse width of 15 ns are not able to produce a significant modification in the surface composition with the in the fluence range (0.4-0.8) J/cm^2. This conclusion is inferred from the relatively small values of R_{pol}, which are in the (189-512) $k\Omega cm^2$ range. Observed increase in the R_{pol} value compared to the untreated AA surface may be explained as the laser-induced growth of a thin aluminum oxide layer on the metal surface.

Increasing the laser fluence above the threshold for preferential copper removal (1.2 to 2 J/cm^2) significantly increases polarization resistance from 1206 to 2876 $k\Omega cm^2$ respectively. Analogously, E_{pit} increased from –0.280 V to +0.05 V, indicative of improved corrosion resistance characteristics. This phenomenon may be explained by complementary laser-induced copper ablation and growth of the dense aluminum oxide layer caused by irradiation using moderate laser fluences.

Irradiation using higher fluences, for example, 3 J/cm^2, was found to decrease corrosion resistance characteristics, presumably due to migration of bulk copper atoms to surface sites. Surface morphology at the higher fluences was found to coarsen (Figure 1) and melt oxidation fragments were found to appear at this laser fluence. Multi-pulse induced surface anisotropy,

absorption variation, surface stress, and thermal quenching differences lead to a complexity in the elementary removal and redistribution that made the surface property complicated.

D. Conclusions

Surface modification of 2024-T3 AA with nanosecond pulse laser irradiation produces two complementary surface processes: preferential copper removal and growth of a dense aluminum oxide layer on the alloy surface. Surface modifications using low laser fluences (0.4-0.8) J/cm^2, were not able to extract significant copper concentrations from the aluminum alloy surface. Elevated corrosion resistance characteristics were not observed for low laser fluences.

Increasing the laser fluence into the 1.2 to 2 J/cm^2 range was found to promote preferential copper removal and an increase in corrosion resistance characteristics, as R_{pol} was found to increase to 2876 kΩcm^2. Analogously, E_{pit} increased from –0.280 to 0.05 V upon increasing the laser fluence from 1.2 to 2 J/cm^2, indicating improved corrosion characteristics. This phenomenon was postulated to be due to complementary laser induced copper removal and growth of a dense aluminum oxide layer.

Table 1: Electrochemical characteristics derived from PDS.

Composition	Laser Fluence, J/cm^2	Number of Pulses	$I_{corr} \times 10^7$, A/cm^2	E_{corr}, mV	E_{pit}, mV	R_{corr}, $k\Omega cm^2$
2024-T3 AA	---	---	5.0	-0.682	-0.509	49
0.25 M $K_2Cr_2O_7$	---	---	0.16	-0.390	-0.09	1500
2024-T3	1.2	20	0.7	-0.680	-0.26	359
2024-T3	1.2	100	0.66	-0.650	-0.22	280
2024-T3	1.2	250	0.87	-0.690	-0.28	287
2024-T3	1.2	500	0.5	-0.695	-0.25	495
2024-T3 AA	0.4	1000	1.0	-0.650	-0.260	250
2024-T3	0.6	1000	1.02	-0.680	-0.280	245
2024-T3	0.8	1000	0.45	-0.675	-0.240	550
2024-T3	1.2	1000	0.2	-0.690	-0.280	1255
2024-T3	2	1000	0.08	-0.660	0.05	3005
2024-T3	3	1000	0.18	-0.675	0.045	1373

Table 2: Electrochemical characteristics derived from EIS.

Composition	Laser Fluence. J/cm^2	Number of Pulses	R_{sol}, $k\Omega cm^2$	C_{dl}, $\mu F/cm^2$	R_{pol}, $k\Omega cm^2$
Bare aluminum	---	---	0.4	10	42
0.25 M $K_2Cr_2O_7$	---	---	0.4	11	1590
2024-T3 AA	1.2	20	0.4	7	348
2024-T3 AA	1.2	100	0.3	4	278
2024-T3 AA	1.2	250	0.3	4	291
2024-T3 AA	1.2	500	0.4	4	469
2024-T3 AA	0.4	1000	0.4	10	189
2024-T3 AA	0.6	1000	0.4	9	224
2024-T3 AA	0.8	1000	0.4	5	512
2024-T3 AA	1.2	1000	0.4	3	1206
2024-T3 AA	2	1000	0.3	2	2876
2024-T3 AA	3	1000	0.4	3	1180

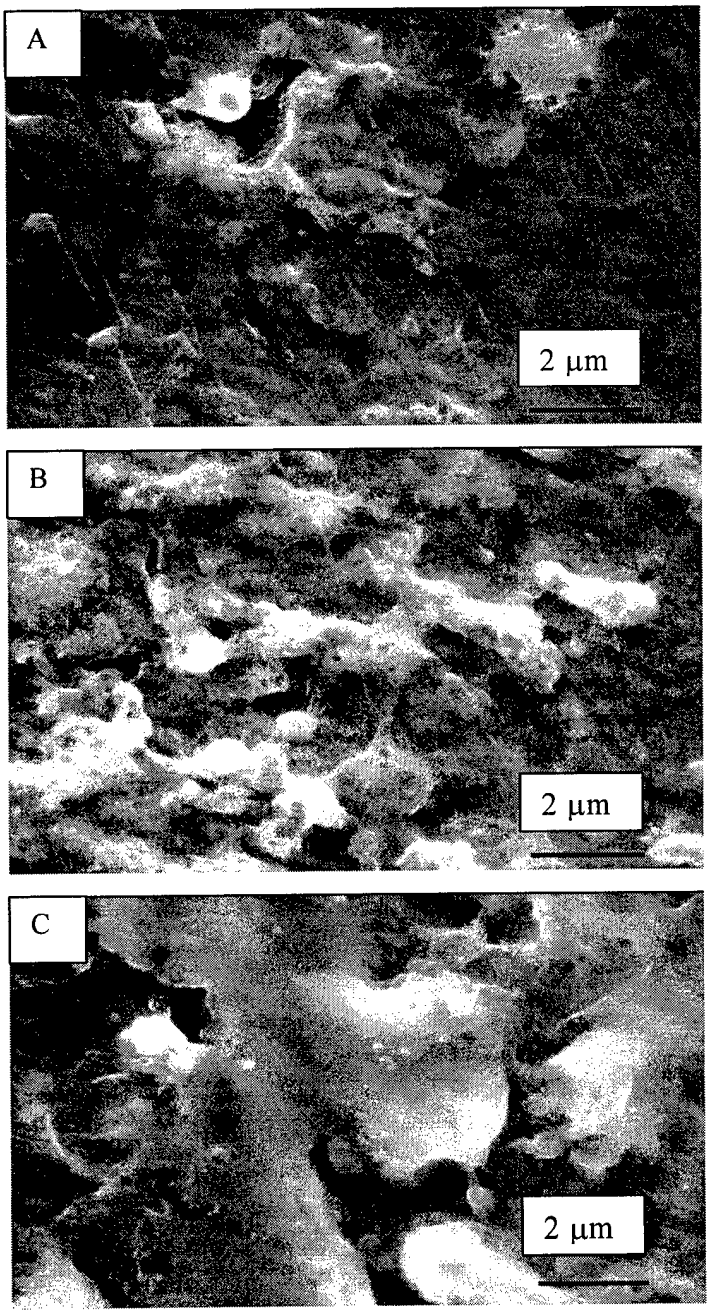

Figure 1. SEM images of aluminum alloy 2024-T3 irradiated with 308 nm/15 ns using the 1000-pulse irradiation at a fluence of (a) 0.8, (b) 1.2, and (c) 3 J/cm^2.

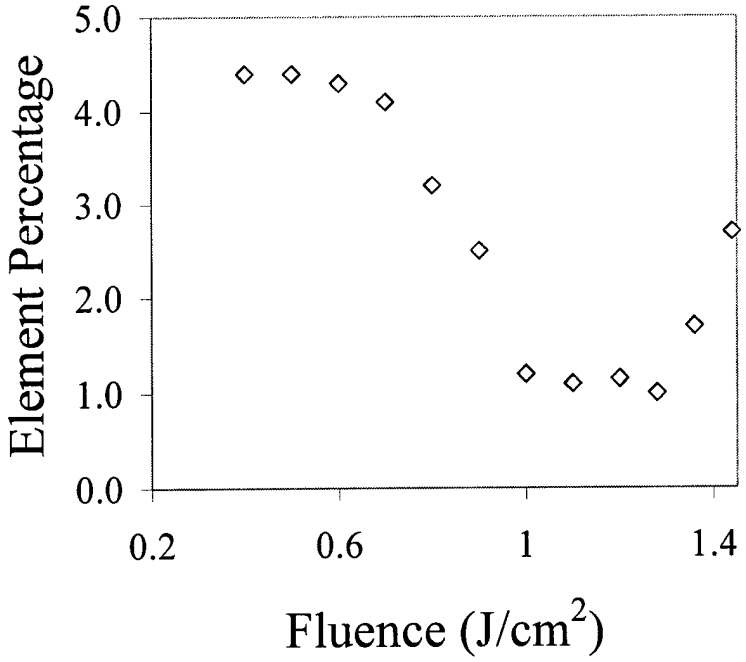

Figure 2. Laser-induced removal of copper as a function of laser fluence using a 15-ns pulsed excimer laser at 308 nm (1000 pulses).

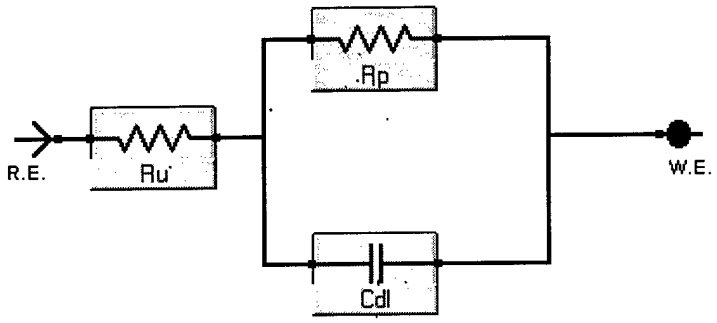

Figure 3. The equivalent circuit used for EIS analysis. R_u denotes solution resistance, R_{pol} denotes polarization resistance, and C_{dl} denotes double layer capacitance.

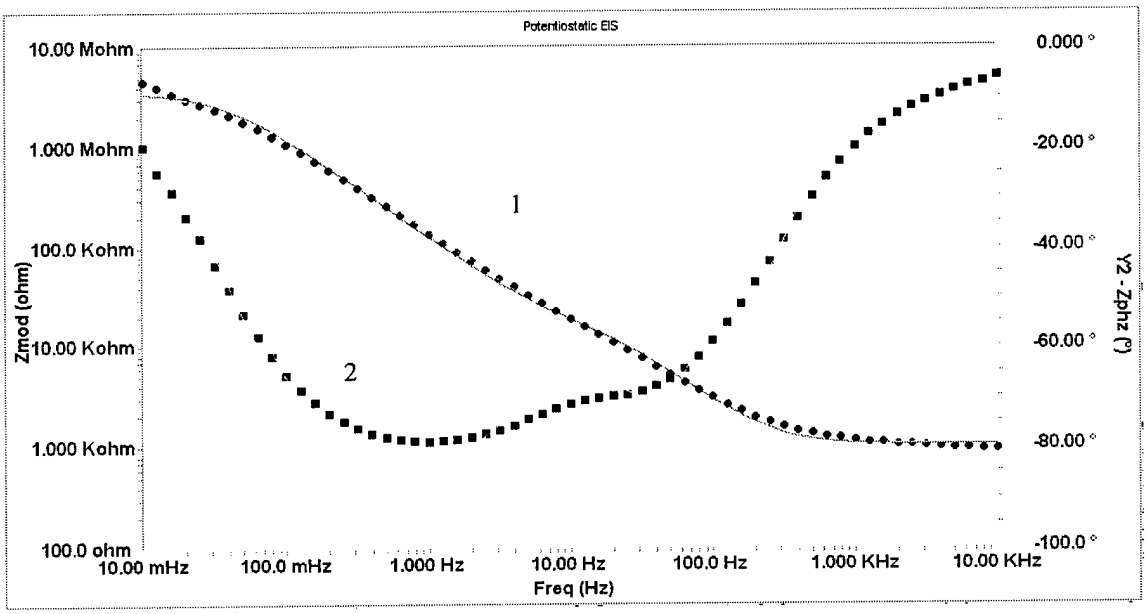

Figure 4: EIS data recorded for AA treated with laser irradiation using a fluence of 1.2 J/cm^2 and 1000 pulses. Curve 1 denotes |Z| vs. frequency. Curve 2 denotes phase angle vs. frequency. The solid line denotes fitting for the Randell model.

II. Sol-Gel Coatings for Corrosion Resistance

A. Introduction

The goal of this portion of the proposed research project is to perform a series of basic and applied materials research studies aimed at developing a technology base that will serve to demonstrate the feasibility of using sol-gel coatings to meet the defined Air Force need for robust, environmentally-compliant replacements for chromate-based conversion coatings. In the present study, organically-modified silicate (Ormosil) films were investigated as corrosion resistant coatings for aluminum alloys.

In recent years, the sol-gel approach has emerged as a versatile method for preparing oxide coatings. Organically modified silicates (Ormosils) are hybrid organic-inorganic materials composed of intimately mixed polymer systems, formed through the hydrolysis and condensation of organically modified silanes with traditional alkoxide precursors producing a silica-based network structure with organic moieties dispersed throughout. ORMOSIL films are of interest for corrosion resistance because they blend the mechanical and chemical characteristics of the comprising organic and inorganic networks. The inorganic components impart durability, scratch resistance, and improved adhesion to metal substrates; the organic components contribute increased flexibility, density, and functional compatibility with organic polymer paint systems. Hybrid films may be tailored to have exceptional durability and adhesion to metals, while providing a dense, flexible barrier to the permeation of water and corrosion initiators. In general, Ormosil coatings:

a. Exhibit excellent adhesion to aluminum alloys
b. Passivate the aluminum alloy substrate against corrosion at a level which meets the current standard established by chromate-based surface treatments

c. Provide a good surface for bonding of primer coatings

d. Exhibit room temperature curing characteristics upon addition of appropriate curing agent

e. Exhibit the potential to be scaleable to comply with applications on the dimensional scale of military aircraft or parts thereof.

Stricter environmental regulations have mandated the near term reduction and/or removal of hexavalent chromium conversion coatings from standard protective paint systems used in aerospace applications. Despite the excellent corrosion resistance properties of chromate conversion coatings, the toxic active ingredient, Cr^{6+}, poses serious human health and environmental concerns[9]. In recent years, a wide variety of novel coating processes have been developed as potential replacements for hexavalent chromium based conversion coatings as described in various reviews[10]. These processes have relied on inorganic molecules that react with the oxidized aluminum surface to form mixed oxides, metal ions that are able to oxidize the metal surface during service life, organic polymers with a high complexing capacity for aluminum surfaces, and inorganic film-forming oxides[11]. Recent developments have included rare earth-based conversion coatings,[12] Co-rich oxide layers,[13] Mn-based conversion coatings,[14] Mo-based conversion coatings,[15] Zr-based conversion coatings,[16] silane-based surface treatments,[17] and trivalent chromium-based conversion coatings.[18]

Coatings derived from organically-modified silicate (Ormosil) materials[19] have found use in a diverse range of high performance applications including enhancement of mechanical, thermal, optical, corrosion resistance and electrical properties of the underlying materials[20]. Organically-modified silicate (Ormosil) coatings have been found to provide good corrosion resistance for metal substrates based on their ability to form dense barriers to the penetration of corrosion

initiators. Review articles by Guglielmi[21], Metroke and Knobbe[22], and Twite and Bierwagen[2d], indicate that sol-gel derived coatings are of interest for corrosion resistance of various metallic substrates.

In recent years, various uses of sol-gel derived coatings have been presented. For example, Kato studied inorganic SiO_2 films derived from $Si(OC_2H_5)_4$-C_2H_5OH-H_2O solutions for the corrosion resistance of aluminum.[23] Van Ooij et al investigated the use of silane-based pretreatments (aminopropyltrimethoxysilane, vinyltrimethoxysilane, 1,2-bis-triethoxysilyl ethane) for the corrosion protection of steel and aluminum alloy substrates[24]. Kasemann and Schmidt found that thermally-cured epoxy silane/bisphenol A coatings exhibited high scratch, abrasion, and corrosion resistance on aluminum, magnesium, and silver[12]. Donley and Vreugdenhal prepared and investigated the use of self-assembled, nano-phase (SNAP) sol-gel derived coatings for the corrosion protection of 2024-T3 aluminum alloy[25]. Our previous works have shown that organic concentration, hydrolysis water ratio, application method and curing agent have a dramatic effect on the corrosion resistance of GLYMO-TEOS Ormosil thin films on 2024-T3 aluminum alloys[26]. Parkhill et al. found that a spray-coated, epoxide modified Ormosil thin film on 2024-T3 aluminum alloy provided several orders of magnitude enhancement in corrosion protection properties compared to the Alodine 1200 type surface pretreatment[27]. Osborne et al found that a series of water-based sol-gel systems exhibited excellent corrosion resistance, hardness, adhesion, and abrasion resistance on aircraft aluminum alloy substrates[28]. Voevodin et al found that an organically-modified zirconate-based film exhibited good corrosion protection of 2024-T3 aluminum alloy[29]. In a related work, Voevodin et al used electrochemical methods to evaluate the corrosion resistance properties of sol-gel derived zirconate-epoxy coatings containing environmentally compliant non-chromate inhibitors[30]. Khobaib et al

evaluated the corrosion protection of a sol-gel based surface pretreatment used in combination with six different primers using electrochemical impedance spectroscopy of coating systems exposed to various environmental conditions, including Harrison's solution, salt fog, and UV light exposure[31]. Yang et al investigated the behavior of a sol-gel derived conversion coating alone and in combination with a polyurethane unicoat[32]. Kachurina et al. and Metroke et al. have investigated the corrosion resistance characteristics of multilayer coatings comprising a conversion coating and an Ormosil thin film.[33]

B. Experimental

1. ORMOSIL Preparation

Several types of ORMOSIL films were investigated during this study, specifically, xVTMOS-yTEOS, xMTMOS-yTEOS, xGLYMO-yTEOS, and aTEOS-bVTMOS-cMTMOS. (x = 60; y = 100-x; a = 30; b = 60; c = 10) In a typical procedure, TEOS and R-Si$(OCH_3)_3$ (R = VTMOS, MTMOS, GLYMO or VTMOS/MTMOS) were placed in a beaker with acidified water. The ORMOSIL solutions were allowed to stir for one hour. Alternatively, a curing agent was added to the siloxane mixture prior to addition of the hydrolysis water. VTMOS denotes vinyltrimethoxysilane; MTMOS denotes 3-(trimethoxysilylpropyl) methacrylate; GLYMO denotes 3-glycidoxypropyltrimethoxysilane; TEOS denotes tetraethylorthosilicate.

2. Aluminum Surface Preparation and Coating Methods:

Aluminum 2024-T3 alloy substrates used for both polarization measurements and salt spray testing were freshly degreased and deoxidized using the following cleaning process. First,

test coupons were wiped with hexanes and methanol. AA substrates were subsequently soaked in aerated Oakite-164 cleaner solution for 15 minutes at 65 °C, and then in Turco Smut-Go or CLEPO 503-ALN deoxidizing solution for 7-10 minutes at 25 °C under rigorous air agitation. Each of these treatments was followed by a thorough rinse for 2 minutes with tap water.

The Ormosil solutions were applied onto cleaned AA by a spray coating technique using an airbrush setup. The coatings were allowed to dry at ambient conditions for at least 24 hours prior to their characterization.

3. Corrosion Resistance:

Corrosion protection properties of the coated AA substrates were evaluated by exposing the substrates to salt fog atmosphere generated from 5 wt.% aqueous NaCl solution at 35 ± 1.7 °C for 168 hours in accordance with ASTM B117 specifications.

4. Polarization Measurements:

Electrochemical measurements were performed using a BAS CV-50-W unit and a three-electrode cell equipped with a platinum counter electrode, a Ag/AgCl/Cl^- (3M KCl) reference electrode and an AA 2024-T3 panel as the working electrode. The latter was either coated or not coated with a film and had an exposed area of 0.36 cm^2. All measurements were conducted in an aqueous 1M NaCl working solution at 25 ± 1 °C. The reported values of potentials both shown in the polarization curves and listed in Table 1 are given relative to the Ag/AgCl/Cl^- reference electrode. Oxygen was removed by purging the solution with purified nitrogen prior to the polarization measurements.

In order to reach steady potential, the electrodes were kept in the working solution for 30 minutes prior to the measurements with the electrical circuit open. Then, the acquisition of polarization curves was started from this open circuit potential, with a constant sweep of 1 mV/sec. Corrosion current values, I_{corr}, reported herein correspond to a 50 mV stretch between the cathodic and anodic parts of the polarization curve. Corrosion resistance was calculated using the equation $R_{corr} = 50mV/ 2I_{corr}$. This differs from the previously described definition of corrosion resistance; however, it allows for the derivation of the parameter R_{corr} for the entire pool of polarization curves collected in this study regardless of their shift along the abscissa. Pitting potentials, E_{pit}, were determined using the criterion that pitting would have occurred by the time the anodic current density of the specimen reached 3×10^{-5} A/cm^2.

5. Solid State NMR Analysis

Solid-state NMR experiments were performed on a Chemagnetics CMX-II 300 MHz (7.06 T) spectrometer using a Chemagnetics 300VXP-144 double resonance (H-X) probe for data collection. Resonance frequencies for ^{13}C and ^{1}H were 75.6 and 301.0 MHz, respectively. All peaks are referenced to an external TMS standard. ^{1}H-^{13}C CP/MAS NMR spectra were collected with a quasi-adiabatic cross-polarization pulse sequence using a 1s pulse delay, a 2 ms contact time, a 4 μs pulse width and 10,000 scans. Magic angle spinning was carried out in 5 mm zirconia rotors spinning at 6 kHz.

C. Results and Discussion

1. Structure/Property Relationships

Solid state NMR, potentiodynamic polarization curves, and salt spray analyses have been used to characterize the structure and corrosion resistance properties of sol-gel derived materials. Results of these studies have shown that structural changes in an Ormosil caused by film composition, curing reactions, and hydrolysis water ratio affect the corrosion resistance of the film; these structural changes also affect the sol-gel film's ability to adhere to metal substrates and organic polymer paint systems. Figure 5 shows the structure of organically-modified silanes investigated.

2. Corrosion Resistance

Figure 6(a) shows the results of 168 hour salt spray tests for spray-coated MTMOS-TEOS, VTMOS-TEOS, GLYMO-TEOS, and TEOS-VTMOS-MTMOS Ormosil films. The Ormosil film composition was found to affect the corrosion resistance of the films. Considering the extent of pitting observed, the corrosion protection of all film systems was poor to moderate, with MTMOS-TEOS and TEOS-VTMOS-MTMOS films performing better than the VTMOS-TEOS or GLYMO-TEOS films. Localized pitting was observed as the primary film failure mode. Addition of a curing agent produced a dramatic increase in the corrosion resistance behavior of all Ormosil systems investigated during this study as shown in Figure 6(b). Cured TEOS-VTMOS-MTMOS systems performed best, with very few pits being observed. Cured VTMOS-TEOS films resisted corrosion well, with few localized pits, though more than the TEOS-VTMOS-MTMOS films. MTMOS-TEOS films failed due to small, filiform-like corrosion trails, rather than through localized pit formation. Curing of GLYMO-TEOS films improved corrosion resistance marginally, though film failure was due to localized pit formation.

In order to confirm the corrosion resistance trends observed in the salt spray test, electrochemical analysis using potentiodynamic polarization curves was conducted. Table 3 shows the results of potentiodynamic polarization curve analysis for Ormosil films. There is a significant increase in corrosion protection afforded by coating the aluminum alloy with an Ormosil film as indicated by an increase in corrosion resistance, R_{corr}, from 2 $k\Omega cm^2$ for bare aluminum to (28 to 79) $k\Omega cm^2$ for AA coated with an Ormosil films. Addition of the curing agent to the Ormosil lead to a further increase in R_{corr} to 125-198 $k\Omega cm^2$ for MTMOS-TEOS, VTMOS-TEOS, and TEOS-VTMOS-MTMOS Ormosil films. Addition of the curing agent to GLYMO-TEOS does not improve significantly the protection ability of Ormosil films. The corrosion potentials for all cured and non-cured Ormosil films are in the same range (-500 to -427)mV. Similarly, there is not a significant difference in E_{pit} values, for all cured and non-cured Ormosil films as they are in the same range (-438 to -300) mV.

3. Ormosil Structural Characterization

In order to further understand the electrochemical and salt spray corrosion resistance trends and the enhancement of corrosion resistance by addition of the curing agent, solid state NMR spectra were recorded of the dried Ormosils prepared in this study. Results of ^{1}H-^{13}C CP/MAS NMR experiments are shown in Figure 7. The ^{1}H-^{13}C CP/MAS NMR spectra of VTMOS-TEOS, MTMOS-TEOS, GLYMO-TEOS, and TEOS-VTMOS-MTMOS Ormosils prepared without addition of the curing agent are provided as a reference.

a. *MTMOS-TEOS Ormosils*

The ^{1}H-^{13}C CP/MAS NMR spectrum of the MTMOS-TEOS Ormosil contains peaks due to the methacrylate functionality at 169.2, 137.7, 126.8, 67.1, 18.2, and 8.5 ppm. Addition of the curing agent produced two new peaks at 27.5 and 11.5 ppm, due to the curing agent. No new peaks were observed which could be assigned to crosslinking reactions between the methacrylate functionalities and the curing agent. The enhancement in corrosion resistance upon addition of the curing agent is postulated to be due to the increased hydrophobicity imparted by the presence of the propyl group on the curing agent. This, combined with the pendant methacrylate groups dispersed throughout the Ormosil film, produces a hydrophobic film, with good water-repellent properties and enhanced corrosion resistance.

b. *VTMOS-TEOS Ormosils*

The ^{1}H-^{13}C CP/MAS NMR spectrum of the VTMOS-TEOS Ormosil contains peaks due to the vinyl functionality at 138.3 and 130.1 ppm. Additional peaks are observed in the 0-35 ppm region, indicating small contributions from possible acid-catalyzed homopolymerization of vinyl groups. Addition of the curing agent produced a decrease in the intensities of the vinyl peaks, indicating some, but not all vinyl groups react during the curing step. The 0-40 ppm region increases in intensity and complexity after addition of the curing agent. New peaks are observed at 35.2, 23.4, 27.6, and 12.3 ppm. The two latter peaks are due to carbon atoms on the curing agent. The two new peaks at 35.2 and 23.4 ppm may be attributed to crosslink products formed between the vinyl groups and the curing agent. While these results are preliminary, we expect the presence of crosslinks to lead to densification of the Ormosil films, and also to an increase in the hydrophobicity of the film. These structural changes may combine to enhance the corrosion resistance of the VTMOS-MTMOS Ormosil films after curing.

c. *TEOS-VTMOS-MTMOS Ormosils*

TEOS-VTMOS-MTMOS Ormosils contain both vinyl and methacrylate functional groups. Changes in the ^{1}H-^{13}C CP/MAS NMR spectrum for TEOS-VTMOS-MTMOS Ormosils are similar to those observed for the VTMOS-TEOS system. There is a decrease in the intensities of the vinylic carbon peaks at 138.3 and 130.1 ppm, as well as new peaks at 35.7, 27.5, 23.3, and 12.0 ppm, characteristic of the vinyl-crosslinking reactions previously described. This indicates that the enhanced corrosion protection in this system may be caused by densification due to curing reactions and increased hydrophobicity of the film caused by the presence of both the crosslink and pendant methacrylate functionalities.

d. *GLYMO-TEOS Ormosils*

^{1}H-^{13}C CP/MAS NMR spectra contain peaks at 51.0 and 44.0 ppm peaks due to the epoxide ring. Curing near completely removed these peaks, indicating the crosslinking reaction occurs at the epoxide groups. Peaks from the expected reaction products are not dominant in the NMR spectrum of the cured ORMOSIL. A new peak appears to be superimposed on the doublet centered at approximately 72 ppm, indicating possible polyether formation. From these results, the mechanism of epoxide curing is unclear.

4. Gelation Times

Observed gelation times for VTMOS-TEOS, MTMOS-TEOS, and GLYMO-TEOS Ormosil systems are shown in Figure 8. For non-cured Ormosils, gelation times were found to increase as the concentration of organics increased. In general, the gelation times were found to

decrease as the organic content increased for cured Ormosils; this behavior indicates a possible interaction of the curing agent with the silicate matrix in addition to the organic functionalities.

5. Corrosion Resistance Characteristics of Other Ormosil Systems

Figure 9 shows results of 168 hour salt spray tests for a wider array of TEOS-VTMOS-TEOS Ormosils using various concentrations of each component. Table 4 shows coating compositions. In all cases, secondary crosslinking reactions produced using a suitable curing agent produced an enhancement in corrosion resistance characteristics, though, in some cases localized pitting was still observed.

6. Failure Mechanisms

For all Ormosil coatings investigated, localized pitting was observed as the primary failure mechanism. Residual porosity or defects in the Ormosil thin film is anticipated to cause the localized pitting. In general, adhesion of the coatings to the metal substrate was excellent and large-scale delamination was not observed.

D. Summary

Results of potentiodynamic polarization curve and accelerated salt spray testing indicate that the addition of a curing agent enhances the corrosion resistance of Ormosil coatings. The corrosion resistance of the cured films under investigation was found to improve GLYMO-TEOS < MTMOS-TEOS < VTMOS-TEOS ≅ TEOS-VTMOS-MTMOS as shown by accelerated salt spray testing and potentiodynamic polarization curve analysis. The observed results may be contribute to structural changes which occur in the Ormosil. For example, characterization using

solid state NMR indicates that the MTMOS-TEOS-modified Ormosils comprise inorganic films with pendant methacrylate and curing agent groups dispersed throughout. This increases the hydrophobicity of the film, leading to better corrosion resistance. The analogous VTMOS-TEOS films contained higher concentrations of crosslinked vinyl functionalities, and presumably, a denser film, and therefore improved corrosion resistance. Combination of the vinyl and methacrylate groups gives a TEOS-VTMOS-MTMOS film which is both partially densified by the presence of the crosslinking, and also increased hydrophobicity, due to the presence of the pendant methacrylate and unreacted vinyl functionalities. In summary, the results of our study indicate that the structure of the Ormosil has a dramatic effect on the corrosion resistance of the coating derived from it.

Table 3: Electrochemical characteristics derived from potentiodynamic polarization curves for Ormosil coatings on 2024-T3 aluminum alloy.

Coating Formula	Mol % Curing Agent	$I_{corr}10_7$, A/cm^2	E_{corr}, mV	E_{pit}, mV	R_{corr}, $k\Omega cm^2$
None	---	182	-719	-540	2
TEOS-VTMOS-MTMOS	---	5.25	-500	-438	48
MTMOS-TEOS	---	3.89	-490	-389	64
VTMOS-TEOS	---	3.16	-438	-346	79
GLYMO-TEOS	---	4.46	-483	-354	28
TEOS-VTMOS-MTMOS	50	1.99	-486	-347	125
MTMOS-TEOS	50	2.24	-541	-369	112
GLYMO-TEOS	50	2.95	-469	-445	42
VTMOS-TEOS	50	1.25	-427	-300	198

Table 4: Compositions of TEOS-VTMOS-MTMOS Ormosils under investigation.

Label	TEOS	VTMOS	MTMOS
FA	50	25	25
FB	50	20	30
FC	50	10	40
FD	50	5	45
FE	50	30	20
FF	50	40	10
FG	50	45	5
FH	30	35	35
FI	30	30	40
FJ	30	20	50
FK	30	10	60
FL	30	40	30
FM	30	50	20
FN	30	60	10
FO	20	40	40
FP	20	30	50
FQ	20	20	60
FR	20	10	70
FS	20	50	30
FT	20	60	20

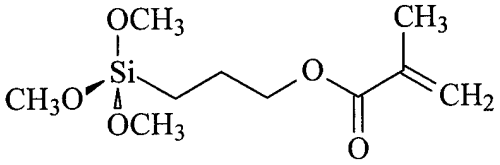

3-(Trimethoxysilyl)propyl methacrylate (MTMOS)

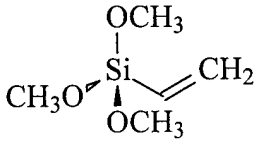

Vinyltrimethoxysilane (VTMOS)

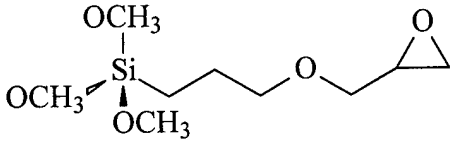

3-Glycidoxypropyltrimethoxysilane (GLYMO)

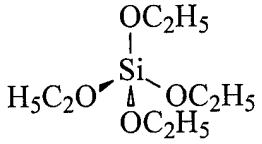

Tetraethylorthosilicate (TEOS)

Figure 5: Silanes investigated during this study.

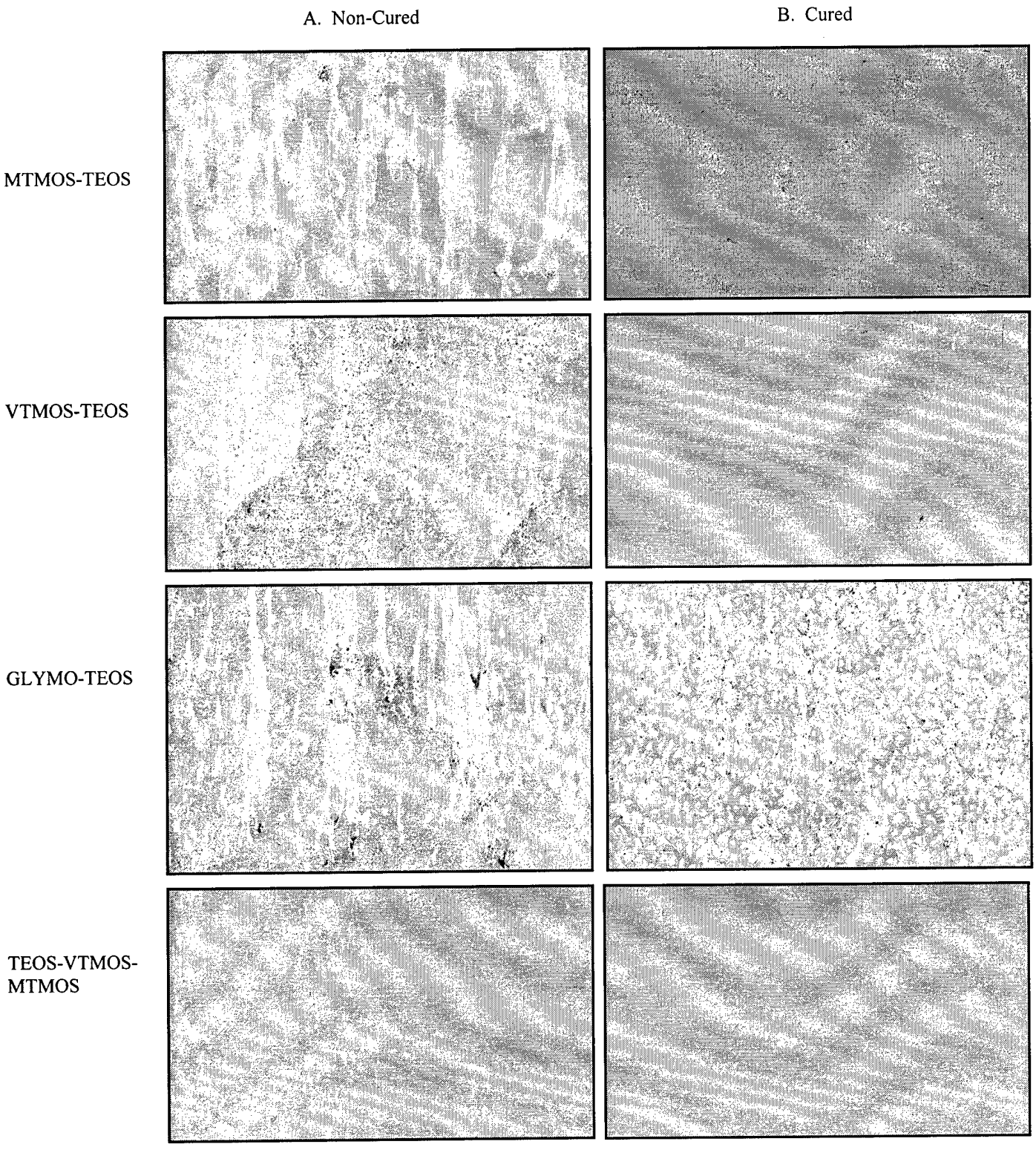

Figure 6: Results of 168 hour salt spray tests for (a) non-cured and (b) cured Ormosils

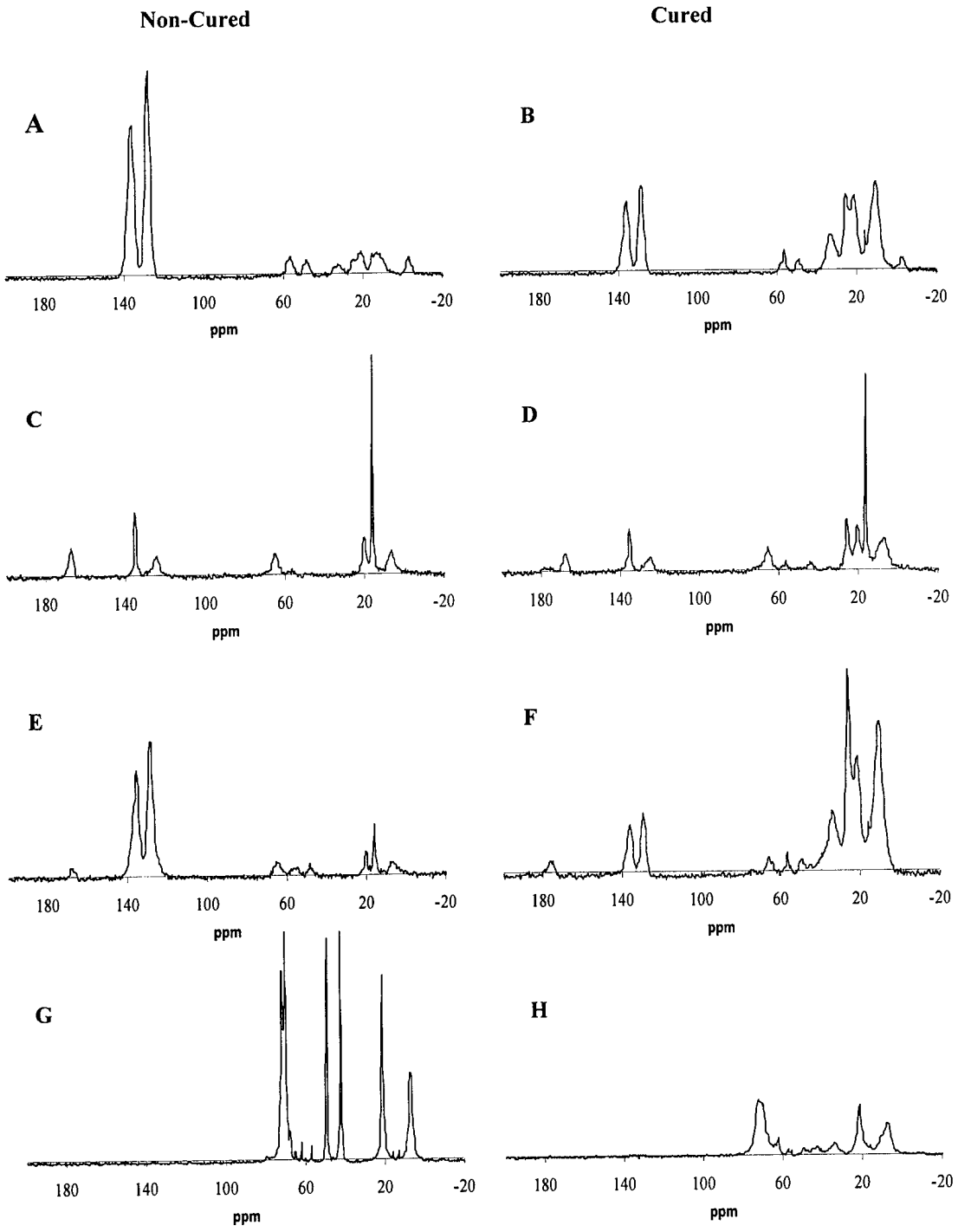

Figure 7. ^{1}H-^{13}C CP/MAS NMR spectra of Ormosils before and after curing. Figures A and B represent VTMOS-TEOS Ormosils; Figures C and D represent MTMOS-TEOS Ormosils; Figures E and F represent TEOS-VTMOS-MTMOS Ormosils. Figures G and H represent GLYMO-TEOS Ormosils.

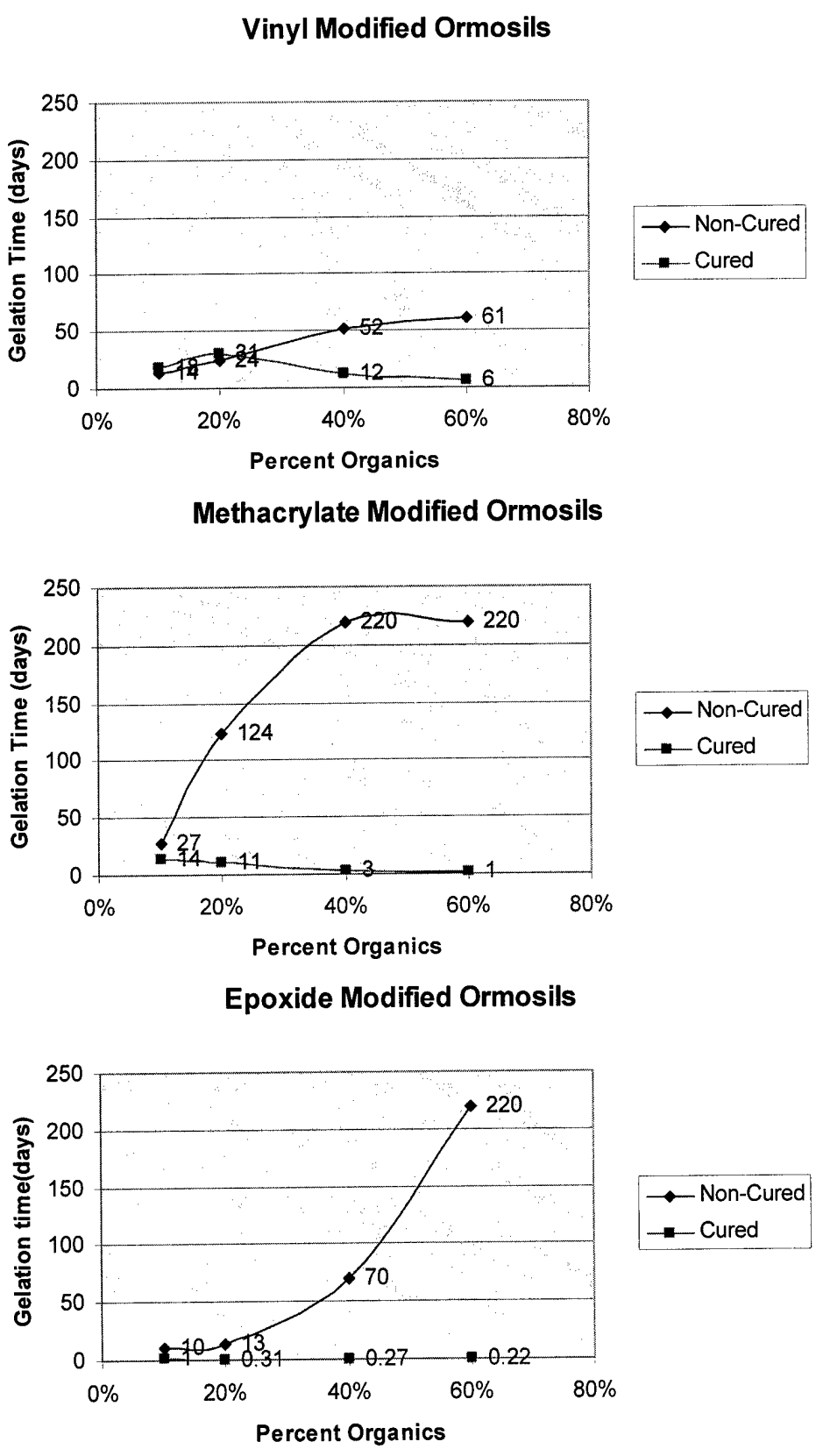

Figure 8: Gelation times for (a) VTMOS-TEOS, (b) MTMOS-TEOS, and (c) GLYMO-TEOS Ormosil systems.

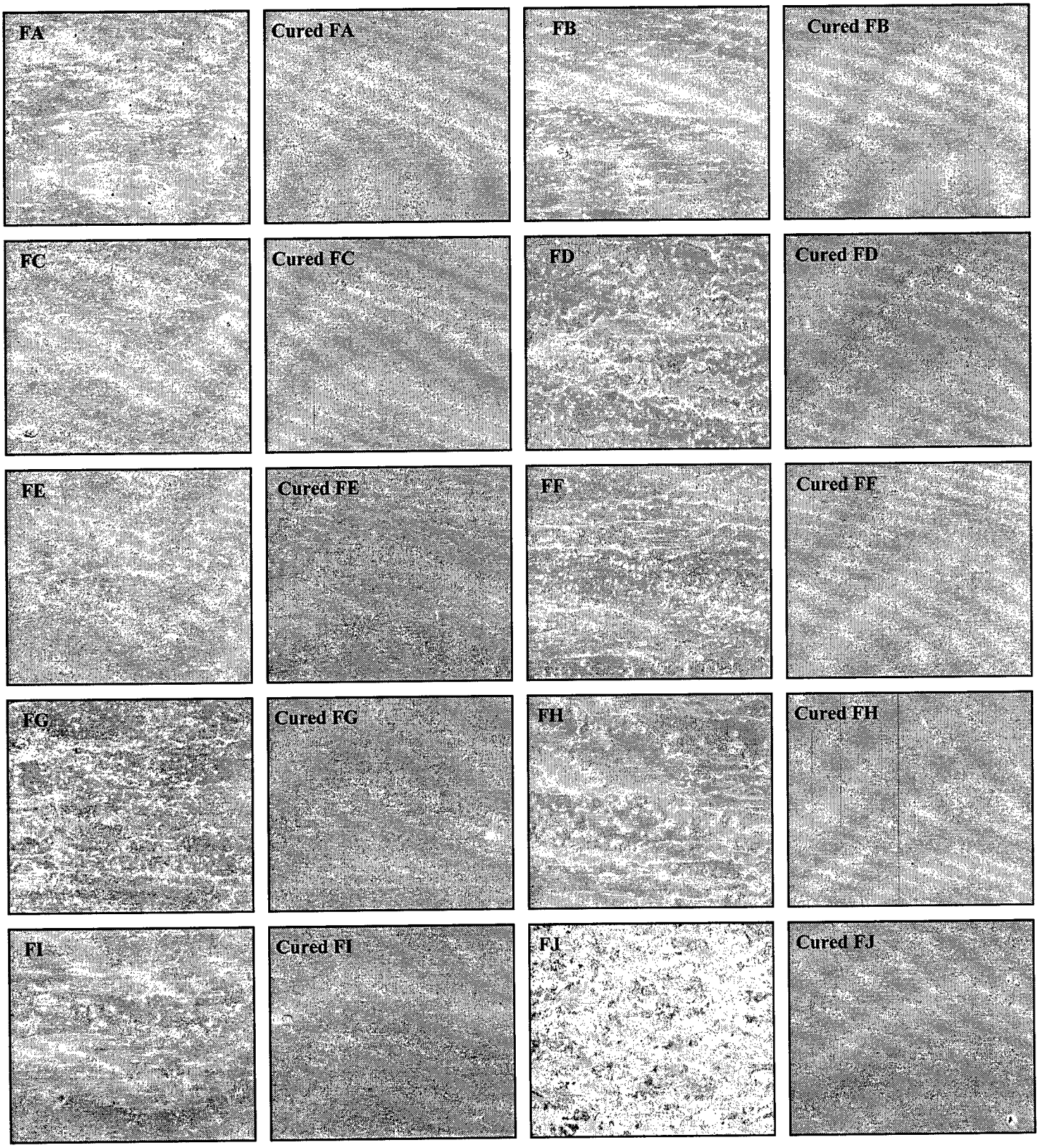

Figure 9: Results of 168 hour salt spray testing for various TEOS-VTMOS-MTMOS Ormosil thin films.

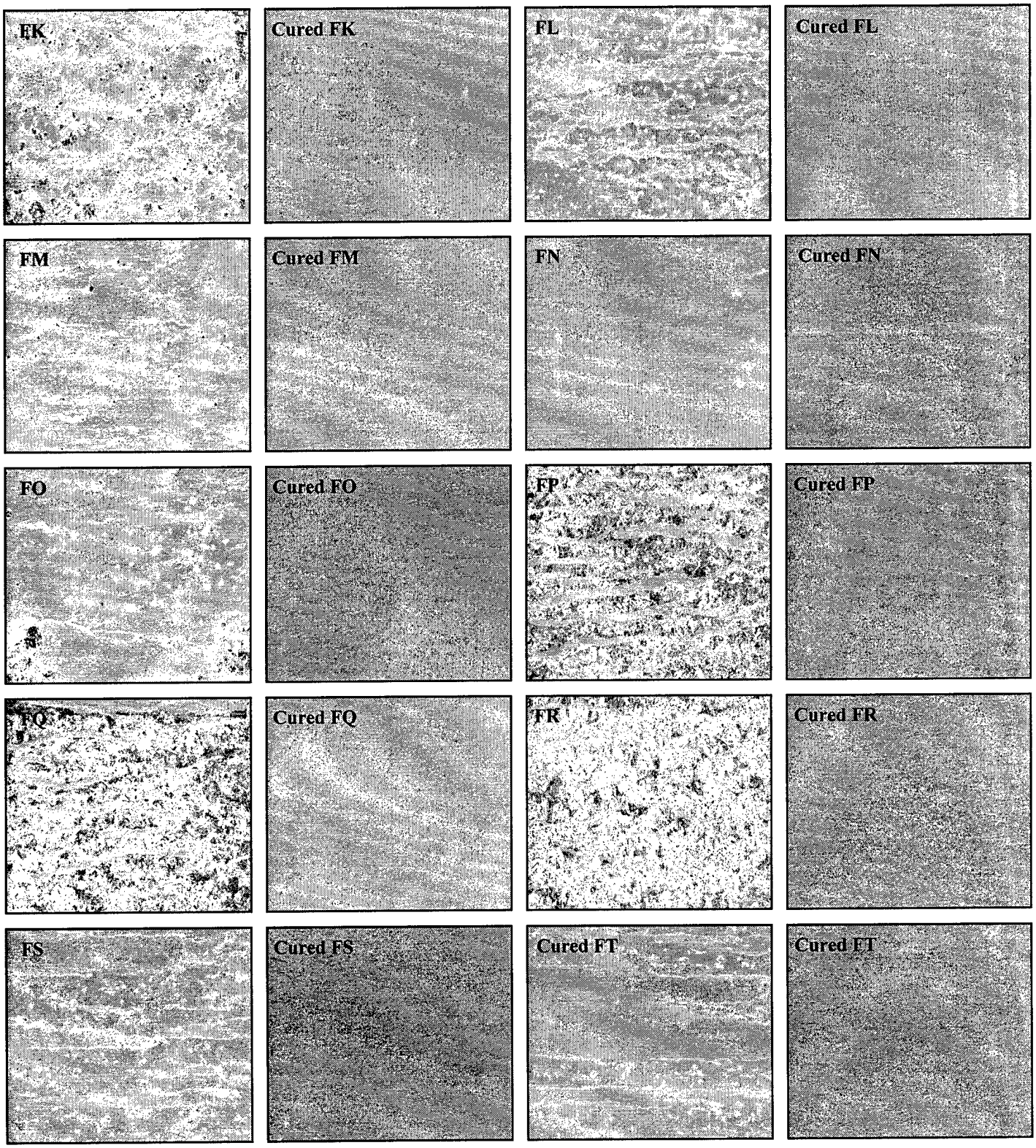

Figure 9, continued.

References

[1] J. Vereecken, G. Goeminne, I. De Graeve, H. Terryn., *The 13th International Corrosion Congress*, paper 213/1-5, (1996).

[2] K. Dou, Robert L. Parkhill, Jack Wu, and Edward T. Knobbe., *IEEE Journal of Selected Topics In Quantum Electronics,* 7 (2001).

[3] *Principles and Prevention of Corrosion*, D.A. Jones, ed.; Macmillian Publ. Co.: New York, NY, (1992).

[4] R. Twite, S. Balbyshev, and G. Bierwagen, Proc. Symposium on Environmentally Acceptable Inhibitors and Coatings, Special Publication of the Electrochemical Society, 95-16 (1997) 202.

[5] Ilevbare, G.O., Scully, J.R., Yuan, J., Kelly, R.G., *Corrosion*, 56 (2000) 227.

[6] R.C. Bacon, J.J. Smith, and F.M Rugg, Ind. Eng. Chem., 40 (1948) 161.

[7] "Standard Practice for Conventions Applicable to Electrochemical Measurements in Corrosion Testing," ASTM G3.

[8] L.Levela, J.Chin, B.del Amo., *Progress in Organic Coatings*, 36 (1999) 211-216.

[9] N.J. Sax, Dangerous Properties of Industrial Materials, 5th ed. Van, New York, 1993.

[10] (a) Nylund, A., *Aluminum Transactions*, 2 (2000) 121; (b) Smith, C.J.E., Baldwin, K.R., Garrett, S.A., Gibson, M.C., Hewins, M.A.H., Lane, P.L., *ATB Metallurgie*, 37 (1997) 266; (c) Puippe, J., *Galvanotechnik.*, 90 (1990) 3003; (d) Twite, R.L., and Bierwagen, G.P., *Progress in Organic Coatings*, 33 (1998) 91; (e) Hinton, B.R., *Metal Finishing*, 89 (1991) 15.

[11] Roland, W., Kresse, J., *ATB Metallurgie*, 37 (1997) 89.

[12] (a) Hinton, B.R.W., *J. Alloys Compd.* 180 (1992) 15; (b) Arnott, D.R., Ryan, N.E., Hinton, B.R.W., Sexton, B.A., Hughes, A.E., *Appl. Surf. Sci.*, 22 (1985) 236; (c) Morris, E., Stoffer, J.O., O'Keefe, T.J., Yu, P., Lin, X., *Polymeric Materials*, 81 (1999) 167; (d) Ramanathan, L.V., *Corrosion Prevention & Control*, 4 (1998) 87.

[13] Schriever, M.P., U.S. Patent 5,551,994 (Sept. 3, 1996).

[14] (a) Danilidis, I., Sykes, J.M., Hunter, J.A., Scamans, G.M., *Surface Engineering*, 15 (1999) 401; (b) Srinivasan, P.B., Sathiyanarayanan, S., Marikkannu, C., Balakrishnan, K., *Corrosion Prevention & Control*, April (1995) 35.

[15] Rangel, C.M., Simões, A., Newman, R.C., *Portugaliæ Electrochimica Acta,* 15 (1997) 383.

[16] Schram, T., Goeminne, G., Terryn, H., Vanhoolst, W., Van Espen, P., *Trans. I.M.F.*, 73, 91 (1995); (b) F. Pearlstein, V.S. Agarwala, *Plating and Surface Finishing*, 81 (1994) 50.

[17] (a) van Ooij, W.J., Zhang, C., Zhang, J.W., Yuan, W., *Electrochemical Society Proceedings*, 97-41 (1998) 222; (b) van Ooij, W.J., Song, J., Subramanian, V., *ATB Metallurgie*, 37 (1997) 137; (c) Child, T.F. and van Ooij, W.J., *Trans. IMF.*, 77 (1999) 64; (d) Subramanian, V. and van Ooij, W.J., *Surface Engineering*, 15 (1999) 168; (e) van Ooij, W.J. and Child, T., *ChemTech*, 28 (1998) 26.

[18] Delaunois, F., Poulain, V., Petitjean, J.P., *ATB Metallurgie*, 37 (1997) 106.

[19] (a) Schmidt, H.K., *Mater. Res. Soc. Symp. Proc.*, 180 (1990) 961; (b) J.D. Mackenzie, *J. Sol-Gel Sci. Technol.* 1 (1994) 81.

[20] R. Kasemann, H. Schmidt, *New J. Chem.*, 18 (1994) 1117.

[21] Guglielmi, M., *J. Sol-Gel Sci. Tech.*, 8 (1997) 443.

[22] Metroke, T.L., Parkhill, R.L., Knobbe, E.T., *Prog. Org. Coatings* 41, (2001) 233.

[23] (a) Kato, K., *J. Mater. Sci.,* 28 (1992) 1445; (b) Kato, K., *J. Mater. Sci.,* 28 (1993) 4033.

[24] (a) van Ooij, W.J., Zhang, C., Zhang, J.W., Yuan, W., *Electrochemical Society Proceedings*, 97-41, (1998) 222; (b) van Ooij, W.J., Song, J., Subramanian, V., *ATB Metallurgie*, 37 (1997) 137; (c) Child, T.F. and van Ooij, W.J., *Trans. IMF.*, 77 (1999) 64; (d) Subramanian, V. and van Ooij, W.J., *Surface Engineering*, 15 (1999) 168; (e) van Ooij, W.J. and Child, T., *ChemTech*, 28 (1998) 26.

[25] Donley, M.S., Vreugdenhil, A.J., *J. Coat. Technol.*, 73 (2001) 915.

[26] (a) Metroke, T.L., Parkhill, R.L., Knobbe, E.T., *Mater. Res. Soc. Symp. Proc.*, 576 (1999) 293; (b) Metroke, T.L., Knobbe, E.T., *Mater. Res. Soc. Symp. Proc.*, 628 (2000) CC11.4.1.

[27] Parkhill R.L. Parkhill, E.T. Knobbe and M.S. Donley, *Prog. Org. Coat.*, 41 (2001) 261.

[28] J.H. Osborne, K.Y. Blohowiak, S. R. Taylor, C. Hunter, G. Bierwagen, B. Carlson, D. Bernard, M.S. Donley, *Prog. Org. Coat.*, 41 (2001) 217.

[29] N.N. Voevodin, N.T. Grebasch, W.S. Soto, L.S. Kasten, J.T. Grant, F.E. Arnold and M.S. Donley, *Prog. Org. Coat.*, 41 (2001) 287.

[30] N.N. Voevodin, N.T. Grebasch, W.S. Soto, F.E. Arnold and M.S. Donley, Surface and Coatings Technol., 140 (2001) 24.

[31] Khobaib M. Khobaib, L.B. Reynolds and M.S. Donley, *Surface and Coatings Techol.*, 140 (2001) 16.

[32] Yang X.F. Yang, D.E. Tallman, V.J. Gelling, G.P. Bierwagen, L.S. Kasten and J. Berg, *Surface and Coatings Technol.* 140 (2001) 44.

[33] (a) O. Kachurina, T.L. Metroke, E. Stesikova, E.T. Knobbe, *Journal of Coatings Technology*, 74 (2002) 43-48; (b) T.L. Metroke, O. Kachurina, E.T. Knobbe, *Journal of Coatings Technology*, 74 April (2002) 53-61.